Received: 17 February 2020 | Revised: 17 May 2020 | Accepted: 9 June 2020 | Published on: 9 August 2020

DOI: 10.1002/qj.3850

Quarterly Journal of the Royal Meteorological Society RMetS

RESEARCH ARTICLE

A physically based raindrop–cloud droplet accretion parametrization for use in bulk microphysics schemes

Tanvir Ahmed[1,2] | Han-Gyul Jin[1] | Jong-Jin Baik[1]

[1]School of Earth and Environmental Sciences, Seoul National University, Seoul, South Korea

[2]Department of Physics, Shahjalal University of Science and Technology, Sylhet, Bangladesh

Correspondence
Han-Gyul Jin, School of Earth and Environmental Sciences, Seoul National University, Seoul 08826, South Korea.
Email: hgjin@snu.ac.kr

Funding information
Korea Meteorological Administration, Grant/Award Number: KMI 2020-00710; Seoul National University President Fellowship; The Research Institute of Basic Sciences funded by the National Research Foundation of Korea, Grant/Award Number: NRF-2019R1A6A1A10073437

Abstract

The accretion process in bulk cloud microphysics schemes can be parametrized using the stochastic collection equation (SCE). In this study, the collection efficiency of each raindrop–cloud droplet pair is applied to the SCE to derive a new accretion parametrization that considers a strong variability of accretion rate depending on the cloud droplet and raindrop size distributions. To evaluate the new accretion parametrization (NP), it is implemented into a cloud-resolving model, replacing the original accretion parametrization (OP) based on the continuous collection equation. In the idealized simulations of deep convective clouds, NP predicts overall larger accretion rates and smaller autoconversion rates than OP. The resultant high accretion/autoconversion rate ratio in NP increases the mean raindrop size. This induces faster sedimentation of raindrops that is associated with the earlier onset of surface precipitation and also weakens the evaporation cooling of raindrops that can affect the thermodynamics and dynamics of clouds. Meanwhile, for a given pair of rainwater and cloud water mass contents, the accretion rates in NP have a broad distribution while those in OP are less variant, suggesting that the dependence of the accretion rates on bulk microphysical properties other than the mass contents also needs to be properly considered in accretion parametrizations. Most of the aforementioned differences between the two accretion parametrizations found in the idealized simulations are also found in the real-case simulations of a precipitation event over Bangladesh but the differences are smaller, and the spatial distribution of the accumulated precipitation amount is relatively well predicted by NP compared to OP.

KEYWORDS

accretion parametrization, cloud droplets, cloud-resolving model, raindrops, stochastic collection equation

1 | INTRODUCTION

Cloud-resolving models which explicitly represent moist convective processes have been widely used for weather research and prediction. Cloud-resolving models adopt cloud microphysics schemes to represent grid-scale cloud and precipitation processes. Cloud microphysics schemes are categorized into bin microphysics schemes and bulk microphysics schemes. Because of simpler representations of microphysical processes and much lower computational

cost, bulk microphysics schemes are exclusively employed in operational numerical weather prediction (NWP) models. Predictions using bulk microphysics schemes contain some degree of uncertainty involved with assumptions and limited observations used to represent cloud particle size distributions and parametrize cloud microphysical processes (Johnson *et al.*, 2015). To better understand moist convection through numerical simulations and more accurately predict weather, developments of physically based bulk microphysics schemes need to be continued (Naumann and Seifert, 2016; Paukert *et al.*, 2019).

Kessler (1969) proposed one of the first bulk microphysics schemes for warm clouds. In this scheme, liquid-phase cloud particles are divided into cloud droplets and raindrops, and the rainwater is produced by the autoconversion of cloud droplets into raindrops and the accretion of cloud droplets by raindrops. The importance of the autoconversion and accretion processes in warm clouds has been well investigated through numerical simulations of cumulus and stratocumulus clouds (e.g. Wood, 2005; Morrison and Grabowski, 2007; Michibata and Takemura, 2015). The autoconversion process plays an important role in the initiation of precipitation, and the accretion process mainly contributes to the precipitation intensity (Wu *et al.*, 2018).

For the accretion process, Kessler (1969) parametrized the accretion rate based on a continuous collection concept, which is expressed in a power-law equation and is a function of cloud water and rainwater mixing ratios. After the Kessler's accretion parametrization, various forms of accretion parametrizations have been developed. Tripoli and Cotton (1980) derived the accretion rate in a simple form using the continuous collection equation. Using the results of a large-eddy simulation model with a bin microphysics scheme, Khairoutdinov and Kogan (2000) proposed a simple fitting equation for the accretion rate. Seifert and Beheng (2001) proposed an analytic form of the accretion rate derived from the stochastic collection equation (SCE) by simplifying it with an approximate collection kernel of Long (1974) and corrected using the numerical solution of the full SCE where a more accurate collection kernel than Long's is considered. The SCE gives the time rate of change in the expected value of drop number concentration for a given drop size using a collection kernel. Note that possible fluctuations in drop number concentration around its expected value are not considered in the SCE (Dziekan and Pawlowska, 2017).

Wood (2005) evaluated the widely used accretion parametrizations in the literature through comparison with the numerical solution of the SCE for drizzling stratiform clouds. The accretion parametrizations showed relatively good performance compared to the autoconversion parametrizations, but still exhibited non-negligible biases. The biases may result from the simplicity of the accretion parametrizations. The accretion parametrizations evaluated depend only on cloud water and rainwater mass contents and the functional forms are too simple, making it difficult to represent the variation of the accretion rate with various size distributions of cloud droplets and raindrops; the collection efficiency that varies with the sizes of colliding particles is not considered. Furthermore, the parametrization based on the results of bin microphysics model simulations for one environment (e.g. Khairoutdinov and Kogan, 2000) may yield deviations in simulations for another environment (Morrison and Grabowski, 2007).

The best way to minimize the deviation of the parametrized accretion rate from the numerical solution of the SCE would be to derive the accretion rate analytically from the SCE and avoid unnecessary assumptions. Recently, Lee and Baik (2017) (LB17 hereafter) proposed an elaborate autoconversion parametrization derived analytically from the SCE. In their autoconversion parametrization, the collection efficiency between cloud droplets, which has been often assumed to be a constant, is expressed as a function of individual sizes of colliding cloud droplets. The developed parametrization predicted the autoconversion-related quantities that are closest to those predicted by a bin-based direct SCE solver, compared to other autoconversion parametrizations. As an extension of the autoconversion parametrization of LB17, a similar approach can be applied to the parametrization of the accretion process. An accretion parametrization derived analytically based on the SCE is expected to yield a better representation of the accretion process in reality compared to accretion parametrizations based on the continuous collection equation or based on SCEs that are simplified to some extent, which is the motivation of this study. This new parametrization takes into consideration the collection efficiency of individual raindrop–cloud droplet pairs which is not considered in the simpler previous accretion parametrizations. The new parametrization also considers the contribution of the cloud droplets to the geometric sweep-out volume in the SCE often neglected in the simpler parametrizations.

In this study, a parametrization of the accretion of cloud water by rainwater for use in weather and climate models with bulk microphysics schemes is derived analytically based on the SCE and evaluated. The drop size-dependent collection efficiency obtained using a particle trajectory model (Pinsky *et al.*, 2001) is used for the parametrization. The derivation of a new accretion parametrization is given in Section 2. In Section 3, the new accretion parametrization is evaluated against a conventional accretion parametrization through idealized and real-case simulations using a cloud-resolving model. A summary and conclusions are presented in Section 4.

2 | A NEW ACCRETION PARAMETRIZATION

In this section, a new accretion parametrization is derived. The rate of change in the number concentration of raindrops through the accretion of cloud droplets is described using the SCE:

$$\frac{\partial f_{\mathrm{r}}(m)}{\partial t} = \int_0^m f_{\mathrm{r}}(m-m')K(m-m',m')f_{\mathrm{c}}(m')dm' - \int_0^\infty f_{\mathrm{r}}(m)K(m,m')f_{\mathrm{c}}(m')dm', \quad (1)$$

where $f_{\mathrm{r}}(m)dm$ and $f_{\mathrm{c}}(m)dm$ are the number concentrations of raindrops and cloud droplets in the mass interval $[m,\ m+dm]$, respectively, and K is the collection kernel. Proper rearrangements and substitutions give a simple form of Equation (1) using radii of colliding raindrops and cloud droplets (e.g. Jin *et al.*, 2019):

$$\left.\frac{\partial L_{\mathrm{r}}}{\partial t}\right|_{\mathrm{acc}} = \frac{4}{3}\pi\rho_{\mathrm{w}}\int_0^\infty\int_0^\infty r^3 f_{\mathrm{r}}(R)K(R,r)f_{\mathrm{c}}(r)drdR, \quad (2)$$

where L_{r} is the mass content of rainwater, R and r are the radii of raindrops and cloud droplets, respectively, and ρ_{w} is the density of liquid water. The subscript "acc" refers to the accretion process.

In many bulk microphysics schemes, the size distributions of raindrops and cloud droplets are represented by a three-parameter gamma distribution function (e.g. Walko *et al.*, 1995; Milbrandt and Yau, 2005; Thompson *et al.*, 2008; Morrison and Milbrandt, 2015):

$$f_{\mathrm{r}}(R) = N_{0,\mathrm{r}}R^{\mu_{\mathrm{r}}}\exp(-\lambda_{\mathrm{r}}R), \quad (3a)$$

$$f_{\mathrm{c}}(r) = N_{0,\mathrm{c}}r^{\mu_{\mathrm{c}}}\exp(-\lambda_{\mathrm{c}}r), \quad (3b)$$

where $N_{0,\mathrm{r}}$ and $N_{0,\mathrm{c}}$ are the intercept parameters, μ_{r} and μ_{c} are the shape parameters, and λ_{r} and λ_{c} are the slope parameters. In a double-moment bulk microphysics scheme, the shape parameter should be pre-set or diagnosed if the other two parameters are prognosed. μ_{r} can be set to any constant value or diagnosed using empirical relations (e.g. Cao *et al.*, 2008), but it is set to 0, which yields a traditional exponential size distribution for raindrops, in this study. μ_{c} is diagnosed by an empirical relation $\mu_{\mathrm{c}} = \min\,[15, \mathrm{nint}\,(10^9/N_{\mathrm{c}}+2)]$ following Thompson *et al.* (2008), where N_{c} is the number concentration of cloud droplets (m^{-3}) and nint (x) refers to the nearest integer of x.

The collection kernel K in Equation (2) is given by

$$K(R,r) = \pi(R+r)^2|v_{\mathrm{t,r}}(R) - v_{\mathrm{t,c}}(r)|\eta, \quad (4)$$

where $v_{\mathrm{t,r}}$ and $v_{\mathrm{t,c}}$ are the terminal velocities of raindrops and cloud droplets, respectively, and η is the collection efficiency. The empirical relation of Beard (1976) is a widely used representation of the terminal velocity of liquid water drops (e.g. Pinsky *et al.*, 2001; Khain *et al.*, 2011). Because the empirical relation consists of three different expressions for different size ranges and the expressions are complicated, simpler forms of terminal velocities for raindrops and cloud droplets can be obtained for direct use in a bulk microphysics scheme by nonlinear curve fitting using the terminal velocity relation of Beard (1976) as the reference. The terminal velocity relation for cloud droplets obtained using this method in LB17 and a newly obtained terminal velocity relation for raindrops are given as

$$v_{\mathrm{t,r}} = v_{0,\mathrm{r}}[1-\exp(-\gamma_{\mathrm{r}}R)], \quad (5)$$

$$v_{\mathrm{t,c}} = v_{0,\mathrm{c}}r^2, \quad (6)$$

respectively. Here, the values of $v_{0,\mathrm{r}}$, γ_{r}, and $v_{0,\mathrm{c}}$ are 9.770, 1,097, and 1.0973×10^8, respectively, and $v_{\mathrm{t,r}}$ and $v_{\mathrm{t,c}}$ are in metres per second and R and r are in metres. The obtained terminal velocity relation of raindrops is quite different from the power-law relation that is commonly used in bulk microphysics schemes (Morrison *et al.*, 2005; Lim and Hong, 2010). The power-law relation has an advantage in its simplicity, but its estimation is only valid for a limited size range of raindrops, beyond which a serious deviation takes place (Seifert *et al.*, 2014). If the raindrop terminal velocity is expressed by the asymptotic function, it does not deviate much from realistic values. Figure 1 shows the obtained terminal velocities of raindrops and cloud droplets. Both the terminal velocities agree well with the empirical relation of Beard (1976), except for the overestimation of terminal velocity of very small raindrops (bias of $0.33\,\mathrm{m\cdot s^{-1}}$ for a raindrop with radius of 200 μm) and the underestimation of terminal velocity of very large raindrops (bias of $0.15\,\mathrm{m\cdot s^{-1}}$ for a raindrop with radius of 1,500 μm). In addition, the density factor $(\rho_0/\rho)^{1/2}$, where ρ_0 is the reference air density and ρ is the air density, is multiplied to consider the increase of terminal velocity with the decrease of air density.

The collection efficiency in Equation (4) is given as the product of the collision efficiency and the coalescence efficiency. The coalescence efficiency between large drops and small droplets has not been studied well and has some uncertainty. Beard and Ochs (1995) showed that the estimated coalescence efficiency based on different laboratory experiments can vary much. However, in this study, the coalescence efficiency is assumed to be unity, following the extrapolation of a coalescence efficiency parametrization based on the direct numerical simulation (DNS) results

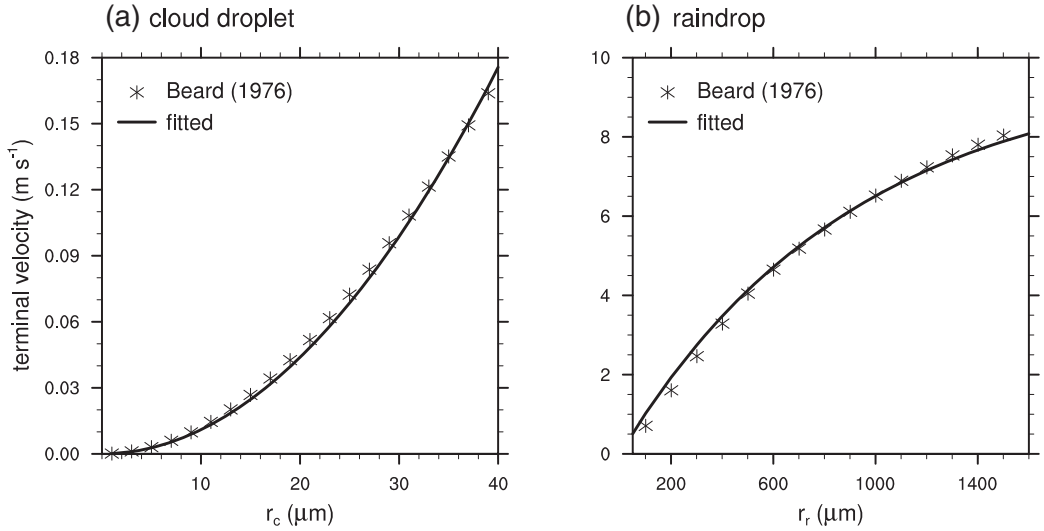

FIGURE 1 Terminal velocities of (a) cloud droplets (Lee and Baik, 2017) and (b) raindrops. The star symbols indicate the terminal velocities from Beard (1976), and the solid lines are the fitted equations

by Straub *et al.* (2010). This seems justifiable because the coalescence efficiency approaches 1 as the Weber number decreases in Straub *et al.* (2010); the Weber number is very small in the accretion regime. The assumption of a coalescence efficiency of 1 means that the collection efficiency is identical to the collision efficiency.

Pinsky *et al.* (2001) performed a detailed study on the collision efficiency using a particle trajectory model and provided the tabulated collision efficiency between raindrops and cloud droplets of various sizes. A limitation of the collision efficiency of Pinsky *et al.* (2001) is that the maximum radius of raindrops considered is limited to 300 μm, because of the challenges associated with describing flow fields around particles for Reynolds numbers greater than 100. The collision efficiency between relatively larger raindrops (~600 μm) and micron-size cloud droplets is provided by Beard and Grover (1974). The collision efficiency of Beard and Grover (1974) is not as reliable as that of Pinsky *et al.* (2001) because the effects of the flow fields around collected drops on the motion of collecting drops are not considered in their study, but it gives a valid estimation for the collision between large raindrops and small cloud droplets. A careful inspection of the collision efficiency of Pinsky *et al.* (2001) for small raindrops and that of Beard and Grover (1974) for relatively large raindrops colliding with micron-size cloud droplets suggests that the collision efficiency is represented well by the following function:

$$\eta = b_0[1 - \exp(-b_1 r)][1 - \exp(-b_2 R - b_3 r)]. \quad (7)$$

A nonlinear fitting using a damped least-squares method to the combination of the two reference collision efficiencies gives the coefficients; the determined values of b_0, b_1, b_2 and b_3 are 1, 246,642 m^{-1}, 3,803 m^{-1}, and 144,650 m^{-1}, respectively. Note that the collision efficiency of Pinsky *et al.* (2001) is considered with a greater weighting to obtain the fitted function because of the greater reliability of the data.

The fitted collision efficiency and its deviation from the reference collision efficiency of Pinsky *et al.* (2001) and Beard and Grover (1974) are shown in Figure 2. Overall, the fitted collision efficiency agrees well with the reference collision efficiency. The collision efficiency for $r < 4$ μm is slightly overestimated, but the gamma size distribution of cloud droplets yields a very small number of cloud droplets in this size range. Thus, the overestimation does not affect the accretion rate significantly except when the number of the very small droplets is unusually large. For a given size of small cloud droplets, the fitted collision efficiency continuously increases as the raindrop size increases, following the tendency in the collision efficiency of Pinsky *et al.* (2001).

Using the above expressions for the size distributions, terminal velocities, and collision efficiency, the analytic expression of Equation (2) can be obtained. Here, the only problem is the absolute value in the collection kernel which makes the analytic integration in Equation (2) challenging. To overcome this problem, an approximation by Gaudet and Schmidt (2005) is employed, where the absolute value of the difference in terminal velocity is approximated as the difference itself. As in Jin *et al.* (2019), box model simulations using a bin-based direct SCE solver confirms that this approximation hardly changes the accretion rate. Then, the accretion rate given

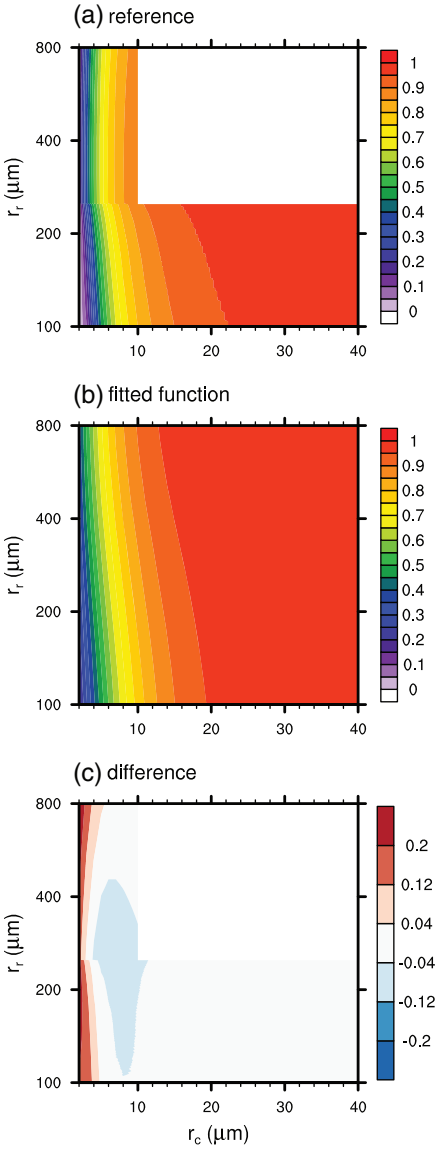

FIGURE 2 (a) The reference collision efficiency between raindrops and cloud droplets which is a combination of the collision efficiencies of Pinsky *et al.* (2001) and Beard and Grover (1974), (b) the fitted collision efficiency, and (c) the fitted collision efficiency minus the reference collision efficiency

by the analytic expression of Equation (2) is

$$\left.\frac{\partial L_r}{\partial t}\right|_{acc} = \frac{4}{3}\pi^2\rho_w\left(\frac{\rho_0}{\rho}\right)^{1/2} N_{0,r}N_{0,c}b_0(v_{0,r}L_1 - v_{0,c}L_2), \quad (8)$$

where

$$L_1 = \sum_{i=0}^{2} a_i \{[\Gamma_1(\lambda_r, \mu_r + 3 - i) - \Gamma_1(\lambda_r + \gamma_r, \mu_r + 3 - i)] \times [\Gamma_1(\lambda_c, \mu_c + 4 + i) - \Gamma_1(\lambda_c + b_1, \mu_c + 4 + i)] - [\Gamma_1(\lambda_r + b_2, \mu_r + 3 - i) - \Gamma_1(\lambda_r + b_2 + \gamma_r, \mu_r + 3 - i)] \times [\Gamma_1(\lambda_c + b_3, \mu_c + 4 + i) - \Gamma_1(\lambda_c + b_1 + b_3, \mu_c + 4 + i)]\}, \quad (9a)$$

$$L_2 = \sum_{i=0}^{2} a_i \{\Gamma_1(\lambda_r, \mu_r + 3 - i) \times [\Gamma_1(\lambda_c, \mu_c + 6 + i) - \Gamma_1(\lambda_c + b_1, \mu_c + 6 + i)] - \Gamma_1(\lambda_r + b_2, \mu_r + 3 - i) \times [\Gamma_1(\lambda_c + b_3, \mu_c + 6 + i) - \Gamma_1(\lambda_c + b_1 + b_3, \mu_c + 6 + i)]\}, \quad (9b)$$

with a_i given as $(a_0, a_1, a_2) = (1, 2, 1)$. $\Gamma_1(\lambda, s)$ is defined as

$$\Gamma_1(\lambda, s) = \frac{\Gamma(s)}{\lambda^s}, \quad (10)$$

where Γ is the gamma function and $s > 0$. The variation of the size distribution parameters that represents the variation of the cloud droplet and raindrop size distributions yields the variation of the accretion rates. Mass conservation yields the following relation:

$$\left.\frac{\partial L_c}{\partial t}\right|_{acc} = -\left.\frac{\partial L_r}{\partial t}\right|_{acc}, \quad (11)$$

where L_c is the mass content of cloud water.

The rate of change in the cloud droplet number concentration due to the accretion process is given by

$$\left.\frac{\partial N_c}{\partial t}\right|_{acc} = -\int_0^\infty \int_0^\infty f_r(R)K(R, r)f_c(r)drdR. \quad (12)$$

Following the procedure of obtaining the analytic expression of the accretion rate Equations (8)–(9), one can show that Equation (12) is expressed as follows:

$$\left.\frac{\partial N_c}{\partial t}\right|_{acc} = -\pi\left(\frac{\rho_0}{\rho}\right)^{1/2} N_{0,r}N_{0,c}b_0(v_{0,r}N_1 - v_{0,c}N_2), \quad (13)$$

where

$$N_1 = \sum_{i=0}^{2} a_i \{[\Gamma_1(\lambda_r, \mu_r + 3 - i) - \Gamma_1(\lambda_r + \gamma_r, \mu_r + 3 - i)] \times [\Gamma_1(\lambda_c, \mu_c + 1 + i) - \Gamma_1(\lambda_c + b_1, \mu_c + 1 + i)] - [\Gamma_1(\lambda_r + b_2, \mu_r + 3 - i) - \Gamma_1(\lambda_r + b_2 + \gamma_r, \mu_r + 3 - i)] \times [\Gamma_1(\lambda_c + b_3, \mu_c + 1 + i) - \Gamma_1(\lambda_c + b_1 + b_3, \mu_c + 1 + i)]\}, \quad (14a)$$

$$N_2 = \sum_{i=0}^{2} a_i \{\Gamma_1(\lambda_r, \mu_r + 3 - i) \times [\Gamma_1(\lambda_c, \mu_c + 3 + i) - \Gamma_1(\lambda_c + b_1, \mu_c + 3 + i)]$$

$$- \Gamma_1(\lambda_r + b_2, \mu_r + 3 - i)$$
$$\times [\Gamma_1(\lambda_c + b_3, \mu_c + 3 + i)$$
$$- \Gamma_1(\lambda_c + b_1 + b_3, \mu_c + 3 + i)] \Big\}. \quad (14b)$$

The raindrop number concentration is not affected by the accretion process.

Note that the existence of the terms $v_{0,c}L_2$ in Equation (8) and $v_{0,c}N_2$ in Equation (13) stems from the consideration of the cloud droplet terminal velocity in the collection kernel. The advantage of this consideration in the accretion rate estimation is relatively small compared to the advantages of considering the contribution of cloud droplets to the geometric sweep-out area or the individual drop size-dependent collection efficiency instead of the bulk collection efficiency. Also, the bias in the estimated accretion rate caused by ignoring the cloud droplet terminal velocity is small compared to that caused by the overestimation of the terminal velocity of very small raindrops in the fitted function, except for when the mean cloud droplet size is very large. For the cost-efficiency in modelling, $v_{0,c}L_2$ in Equation (8) and $v_{0,c}N_2$ in Equation (13) can be neglected. In this study, however, the full equations are used for the evaluation of the developed parametrization.

3 | EVALUATION THROUGH CLOUD-RESOLVING MODEL SIMULATIONS

The developed accretion parametrization is evaluated through idealized and real-case simulations using a cloud-resolving model. For this, the Weather Research and Forecasting (WRF) model version 3.9.1 (Skamarock *et al.*, 2008) is used. The Thompson–Eidhammer microphysics scheme (Thompson and Eidhammer, 2014) is selected as a microphysics scheme, and the developed accretion parametrization is implemented into the Thompson–Eidhammer microphysics scheme, while the parametrizations of other microphysical processes are unchanged. The Thompson–Eidhammer microphysics scheme uses gamma distribution functions to represent the size distributions of cloud droplets and raindrops, as assumed in the new parametrization. The original parametrization of the accretion of cloud water by rainwater in the Thompson–Eidhammer microphysics scheme is based on the continuous collection equation that neglects the contribution of the size distribution and terminal velocity of cloud droplets to the accretion rate. In addition, the original parametrization mainly adopts the collision efficiency of Beard and Grover (1974) as a bulk collection efficiency which is determined by mean raindrop and cloud droplet radii. In contrast, the new parametrization considers the contribution of cloud droplets to the relative terminal velocity and geometric sweep-out area in the collection kernel (Equation (4)) and uses the individual drop size-dependent collection efficiency instead of the bulk collection efficiency. Also, the collision efficiency is fitted from a combination of the collision efficiency of Pinsky *et al.* (2001) and that of Beard and Grover (1974), which yields greater value compared to when only the collision efficiency of Beard and Grover (1974) is used. In the following subsections, simulations with the original accretion parametrization are also conducted and compared to those with the new accretion parametrization. Hereafter, the new and original parametrizations are called NP and OP, respectively.

3.1 | Idealized simulations

Idealized two-dimensional (2D) mixed-phase deep convective clouds are simulated using the WRF model. The horizontal domain size is 80 km with a grid spacing of 200 m, and the vertical domain size is 20 km with grid spacings ranging from ~180 to ~230 m. At lateral boundaries, the open boundary condition is applied. The sponge layer is located from $z = 15$ km to the domain top. The model is integrated for 120 min with a time step of 2 s.

A composite thermodynamic sounding averaged over June 2014 at Dhaka radiosonde station (23.76°N, 90.38°E), Bangladesh (Figure 3) is used as the initial condition at every grid point to simulate deep convection. June belongs to the active South Asian monsoon period (June to September). The thermodynamic sounding exhibits a very humid state in the lower atmosphere, with a near-surface water vapour mixing ratio of ~20 g·kg^{-1}. For the thermodynamic sounding, the lifting condensation level (LCL) is 0.56 km, the level of free convection (LFC) is 1.75 km, and the equilibrium level (EL) is 13.84 km. The convective available potential energy (CAPE) is 1,174 J·kg^{-1}. No basic-state wind is considered in the idealized simulations. The cloud is initiated using a warm-bubble method.

To examine the impacts of the new accretion parametrization on precipitation, the time series of domain-averaged accumulated surface precipitation amount and surface precipitation rate in NP and OP are compared (Figure 4). In this subsection, the domain average is taken horizontally over 20 km (within ±10 km from the domain centre). The range of the domain average in the x-direction is chosen considering the maximum horizontal extent of the main clouds in the simulations. The surface precipitation (precipitation rate greater than 0.1 mm·h^{-1}) starts at 24 min in NP and 26 min in OP. The

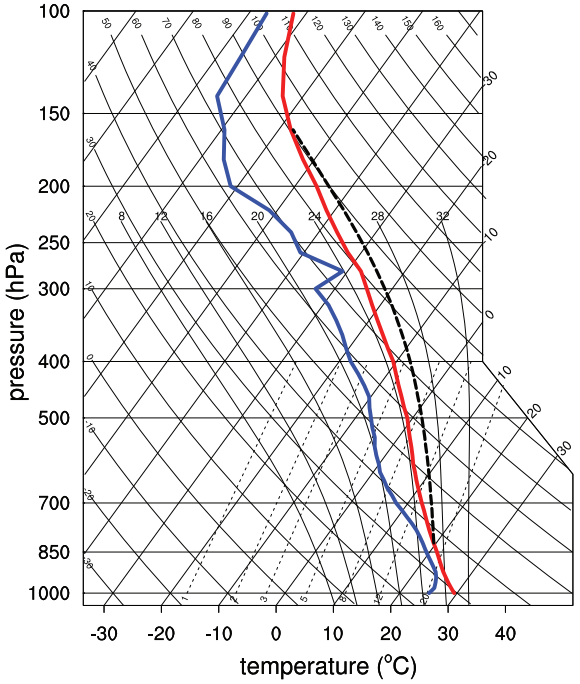

FIGURE 3 Composite of thermodynamic soundings at Dhaka radiosonde station in June 2014. The thick red and blue solid lines indicate the temperature and dew-point temperature, respectively, and the thick black dashed line indicates the temperature of an air parcel lifted moist-adiabatically from the level of free convection

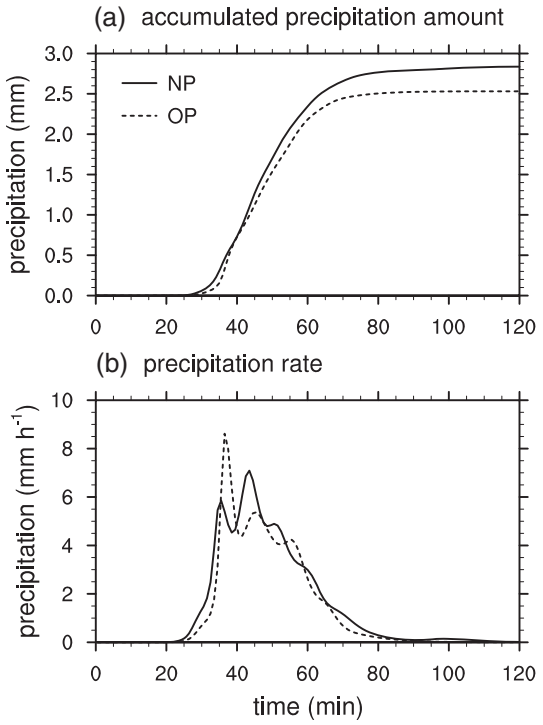

FIGURE 4 Time series of domain-averaged (a) accumulated surface precipitation amount and (b) surface precipitation rate in the idealized simulations with the new and original accretion parametrizations

earlier onset of surface precipitation in NP (2 min earlier) is due to the relatively large accretion rate in NP, which will be shown later. The accumulated surface precipitation amount is consistently larger in NP than in OP until the end of the time integration (Figure 4a). At $t = 120$ min, the accumulated surface precipitation amount in NP is 12% larger than that in OP. The surface precipitation rate is larger in NP than in OP, except for $t = 35$–39 and 54–58 min (Figure 4b). The first peak of the surface precipitation rate appears earlier in NP ($t = 35$ min) than in OP ($t = 36$ min), but its value is smaller in NP (5.8 mm·h^{-1}) than in OP (8.6 mm·h^{-1}).

Figure 5 shows the time- and domain-averaged vertical profiles of hydrometeor mixing ratios and mass-weighted mean radii of cloud droplets and raindrops. The simulated cloud is vertically well developed with a maximum updraught velocity of 12.5 m·s^{-1}, and the cloud top reaches $z = 12.5$ km in NP. Due to effective conversion of cloud water into rainwater, the rainwater mixing ratio is much larger than the cloud water mixing ratio at $z \sim 1.5$–6.2 km (Figure 5a). From $z = 5.0$ km, a little below the freezing level ($z = 5.6$ km), a large amount of snow exists up to the cloud top, and graupel also exists from $z = 4.0$ km to the cloud top in NP. Compared to OP, NP exhibits a larger rainwater mixing ratio at most levels except for $z = 3.6$–5.3 km, while it predicts a smaller cloud water mixing ratio at $z = 0.3$–2.6 km and $z = 4.4$–7.0 km. The snow mixing ratio in NP is much larger than that in OP at $z = 6.5$–10 km, about 94% on average. NP also shows a greater graupel mixing ratio up to $z = 9.2$ km. However, the contribution of the melting process to the production of rainwater mass is relatively small compared to that of the accretion process in these simulations. One of the most prominent differences between NP and OP is shown in the mass-weighted mean radius of raindrops (Figure 5b). The mean raindrop radius in NP is larger than that in OP up to $z = 8.5$ km. Especially at $z = 2.0$–5.0 km, NP exhibits 22% larger mean raindrop radius on average compared to OP. The faster sedimentation of larger-sized raindrops in NP acts as a greater sink of rainwater mass. The smaller rainwater mixing ratio in NP at $z = 3.6$–5.3 km does not indicate that the production processes of rainwater such as the accretion process are relatively weak in NP, but results from the stronger sedimentation process in NP. The time-averaged downward mass flux of rainwater at $z = 3.6$–5.3 km is larger in NP than in OP (not shown). In contrast, the mean cloud droplet radius in NP is smaller than that in OP at most levels below $z = 5.2$ km where the rainwater mixing ratio is large (Figure 5c). The overall larger mean raindrop radius and smaller mean cloud droplet radius in NP still appear

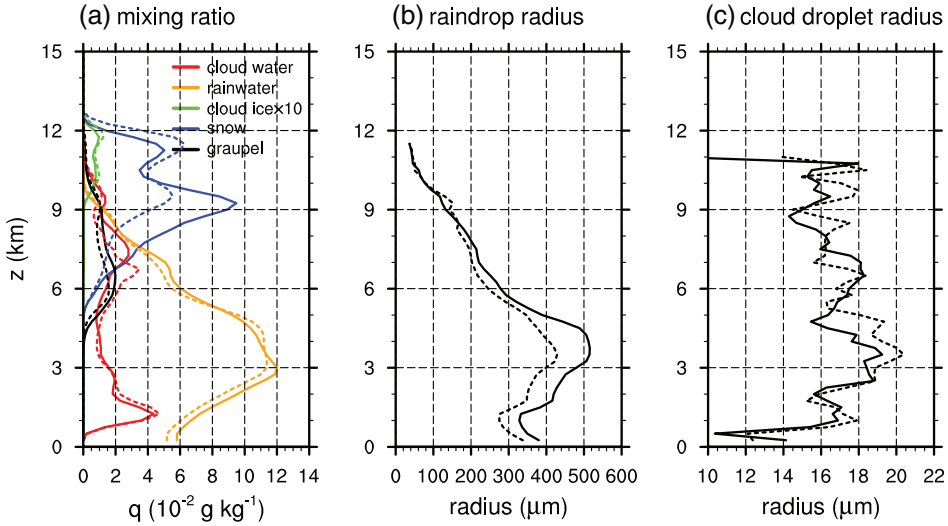

FIGURE 5 Time- and domain-averaged vertical profiles of (a) hydrometeor mixing ratios and mass-weighted mean radii of (b) raindrops and (c) cloud droplets in the idealized simulations with the new (solid lines) and original (dashed lines) parametrizations

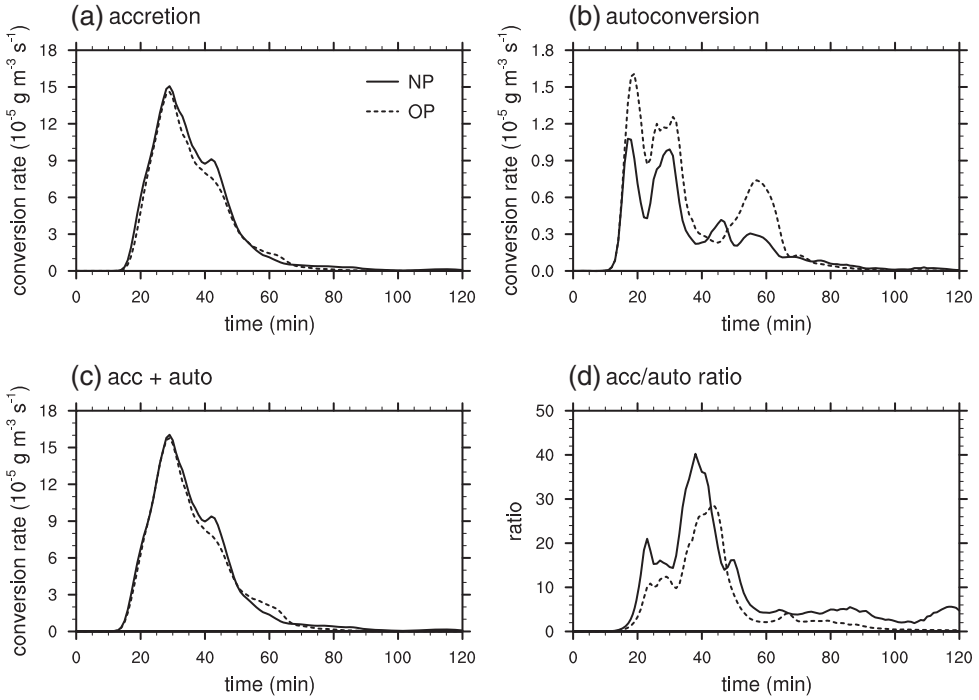

FIGURE 6 Time series of domain-averaged (a) accretion rate, (b) autoconversion rate, (c) the sum of accretion and autoconversion rates and (d) the ratio between accretion and autoconversion rates in the idealized simulations with the new and original parametrizations

when they are averaged only over $t \leq 40$ min during which no ice hydrometeors are present (not shown).

To understand the roles of microphysical processes in the above findings, the time series of domain-averaged accretion and autoconversion rates are shown in Figure 6. Here, the domain average is taken not only horizontally as in Figure 4 but also vertically over $z = 0$–15 km; $z = 15$ km is the bottom height of the sponge layer. The accretion process arises at $t = 13$ min in both simulations (Figure 6a). Since then, NP predicts 56% larger accretion rate on average until $t = 20$ min, compared to OP; this difference looks smaller than its actual value because the accretion rate increases steeply during this time. The difference in the accretion rates becomes smaller and again increases, and the accretion rate in NP remains larger than that in OP until $t = 52$ min. An opposite tendency is predicted when it comes to the autoconversion rates (Figure 6b). As a larger amount of cloud water mass is converted into rainwater through the accretion process in NP, the cloud water mass to be converted into rainwater through the autoconversion process decreases. The sum of the accretion and autoconversion rates is the total rainwater production rate via the warm-rain microphysical processes. Up to $t = 32$ min, the summed rate in NP is not so different from the summed rate in OP; almost the same amount of rainwater mass is produced during this period because the difference in the autoconversion rate between NP and OP largely cancels out the difference in the accretion rate between NP and OP

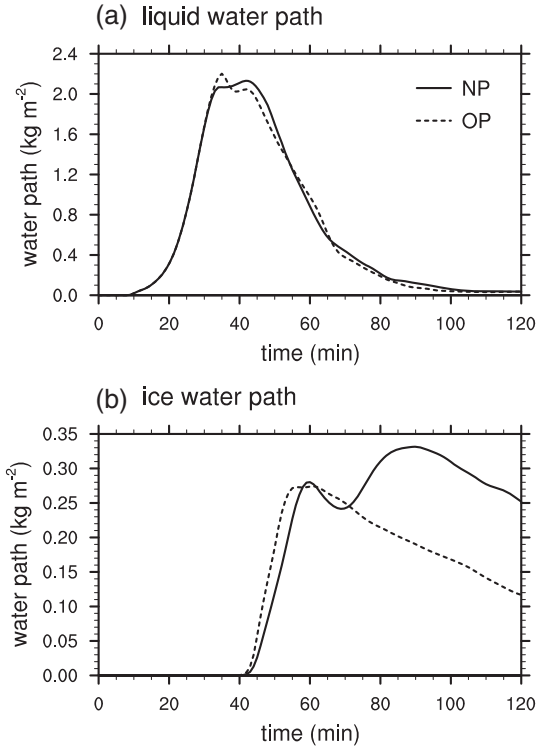

FIGURE 7 Time series of domain-averaged (a) liquid water path and (b) ice water path in the idealized simulations with the new and original parametrizations

(Figure 6c). The difference in the sum of the two rates that arises after $t = 32$ min suggests that there is more cloud water supply in NP possibly driven by other microphysical and dynamical processes, which will be investigated further in this subsection.

The ratio of the accretion rate to the autoconversion rate (acc/auto ratio) is over 10 in NP during $t = 21$–52 min, the relatively convective period (Figure 6d). In this study, the acc/auto ratio is calculated for every time step as the ratio between the accretion and autoconversion rates, and it does not mean the ratio between the accumulated amounts of rainwater produced by the accretion and autoconversion process. Given a similar value of liquid water path (see Figure 7a), NP predicts a much higher acc/auto ratio compared to OP. The accretion process increases the mean size of raindrops by its own nature. The autoconversion process, however, generally decreases the mean size of raindrops because small-sized raindrops are produced as a result of the process. Therefore, the higher acc/auto ratio in NP is responsible for the larger mean raindrop radius shown in Figure 5b. The increased mean raindrop size results in faster sedimentation. The earlier onset of the precipitation in NP (Figure 4b) can be explained by the larger mean raindrop size in NP caused by the higher acc/auto ratio at the early period.

Figure 7 shows the time series of domain-averaged liquid and ice water paths. Here, the liquid water path is the sum of cloud water and rainwater paths, and the ice water path is the sum of cloud ice, snow and graupel water paths. The two simulations exhibit almost the same values of the liquid water path until $t \sim 30$ min; the microphysical processes other than the accretion and autoconversion processes do not make any big difference in the liquid water path between the two simulations during this period (Figure 7a). Although slight differences appear after that, the liquid water path in NP remains close to that in OP for the whole period. On the other hand, the ice water path is very different between NP and OP (Figure 7b). Because of the greater mass conversion of cloud water into rain after $t = 32$ min in NP (Figure 6c), the cloud water mass to be converted into ice hydrometeors through riming decreases in NP, resulting in a slower increase in the ice water path. However, after $t = 75$ min, NP predicts the noticeably larger (79% on average) ice water path compared to OP. The difference in the ice water path could be induced by the difference in the latent heat release between NP and OP.

Figure 8 shows the time- and domain-averaged vertical profiles of latent heating rates and updraught velocity. The condensation and evaporation play important roles at the low and middle levels, and the deposition and sublimation contribute most to the heating rates at the high levels (Figure 8a). NP exhibits stronger net latent heating by condensation and evaporation at $z = 1.6$–4.6 km (Figure 8b), and this is largely due to weaker evaporation cooling there in NP compared to OP (not shown). The large mean raindrop size in NP yields smaller total surface area of raindrops, which weakens the evaporation. Faster sedimentation in NP due to the larger mean raindrop size reduces the time for raindrops to be evaporated, further weakening the evaporation. The stronger latent heating in NP may enhance the convection. The updraught velocity in NP is overall greater than that in OP up to $z = 8.9$ km (Figure 8c). The greater updraught velocity in NP transports more water vapour from lower levels to produce more liquid condensates and transports more cloud water to middle and upper levels which can be converted into ice hydrometeors via freezing and riming processes. These may be responsible for the greater rainwater production rate in NP after $t = 32$ min (Figure 6c) and the greater production rates of the ice hydrometeors in NP (Figure 7b). The greater amount of ice hydrometeors produced in NP can further affect the thermodynamic fields through deposition, sublimation, and riming processes.

To further examine the differences between the two parametrizations, the normalized accretion rates as a function of internal time-scale τ obtained in the idealized

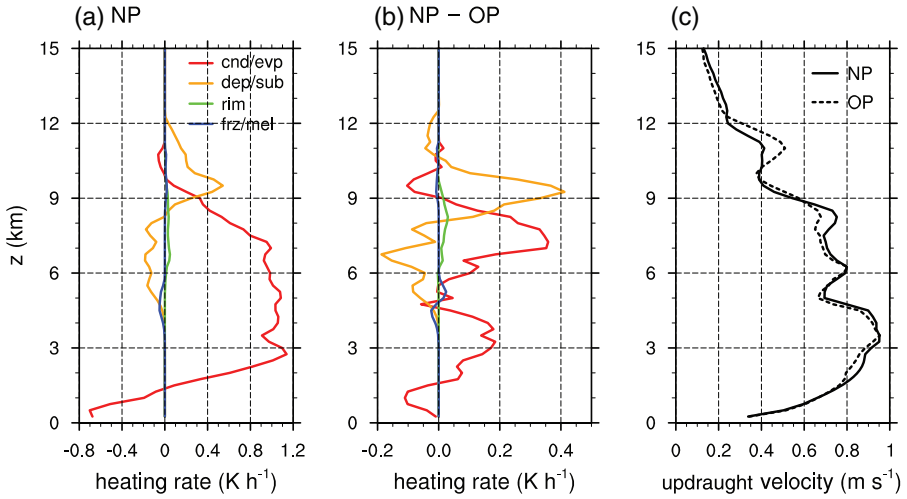

FIGURE 8 Time- and domain-averaged vertical profiles of (a) the heating rates due to condensation/evaporation, deposition/sublimation, riming, and freezing/melting in the idealized simulation with the new parametrization and (b) the differences in the heating rates between the new and original parametrizations. (c) Time- and domain-averaged vertical profiles of updraught velocity ($w > 0.1$ m·s^{-1}) in the idealized simulations with the new and original parametrizations

simulations are plotted (Figure 9). The normalized accretion rate is equivalent to the universal function used in Seifert and Beheng (2001; 2006), which is the accretion rate divided by the product of the rainwater content, cloud water content, and a constant. The internal time-scale τ is the rainwater content divided by the liquid water content, which increases and approaches 1 as the cloud water mass is converted into the rainwater mass. It is noted that in Seifert and Beheng (2001; 2006), the normalized accretion rate is parametrized as a function of τ only. The normalized accretion rates in $t \leq 40$ min and $t > 40$ min which roughly correspond to the liquid-only phase and mixed phase, respectively (see Figure 7), are marked by different colours.

OP exhibits a dense streak of normalized accretion rates which does not vary much (Figure 9b). Because OP is based on the continuous collection equation where the effects of the differences in the cloud droplet size distribution are not considered, the accretion rate tends to depend mostly on the rainwater and cloud water contents. In NP, however, the normalized accretion rates vary largely with τ, and even for the same τ, they are widely distributed (Figure 9a). Additionally, the normalized accretion rates in NP show larger values for the liquid-only phase compared to the mixed phase, while those in OP are not distinguishable for the liquid-only phase and the mixed phase. The fact that the normalized accretion rates have various values for the same τ suggests that the accretion rate strongly depends on some parameters other than the rainwater and cloud water contents, such as the raindrop and cloud droplet number concentrations, and it may not be appropriate to parametrize the accretion rate with the mass contents only. The relatively rapid increase in the normalized accretion rate with τ in NP reflects the relatively rapid increase in the mean raindrop size due to the high acc/auto ratio in NP.

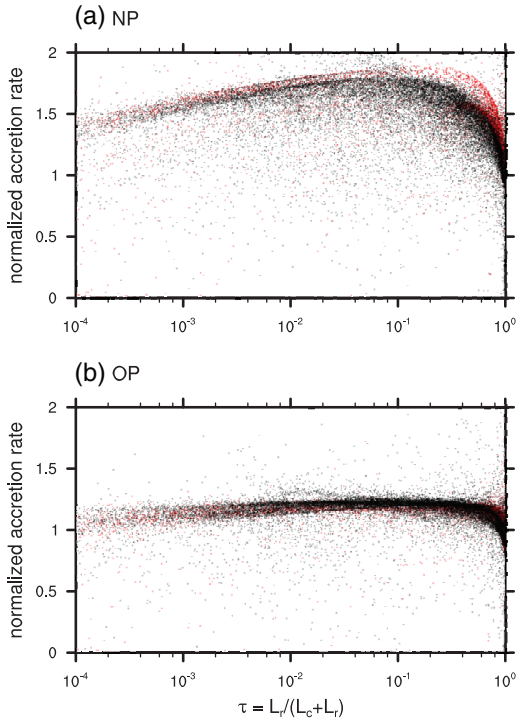

FIGURE 9 Normalized accretion rates as a function of internal time-scale τ in the idealized simulations with the (a) new and (b) original parametrizations. The red dots correspond to the idealized simulation results for $t \leq 40$ min, and the black dots correspond to those for $t > 40$ min

3.2 | Real-case simulations

Real-case simulations are performed to evaluate the new accretion parametrization. Heavy rainfall over Bangladesh from 17 to 23 June 2014 is simulated. During this period, a synoptic trough that was at first located over the west side of the Bay of Bengal moved northeastward. Monsoonal southwesterly winds transported a large amount of

moisture from the Bay of Bengal to Bangladesh, especially to the southeastern region which received the heaviest precipitation (Figure 11c). According to the 35 meteorological stations operated by the Bangladesh Meteorological Department, the maximum 7-day accumulated precipitation amount was 831 mm which was observed at Sandwip (22.48°N, 91.43°E). The precipitation amount for the first 2 days were small, 9% of the total, while that for the last 4 days accounts for 77% of the total.

The WRF model with the Thompson–Eidhammer microphysics scheme (Thompson and Eidhammer, 2014) used in the idealized simulations is again used to simulate the heavy rainfall case but with additional physics parametrizations and different domain configuration. For the physical parametrizations, the Yonsei University (YSU) planetary boundary-layer scheme (Hong *et al.*, 2006), the Betts–Miller–Janjić (BMJ) cumulus parametrization scheme (Janjić, 1994), the unified Noah land surface model (Tewari *et al.*, 2004), the Rapid Radiative Transfer Model (RRTM) long-wave radiation scheme (Mlawer *et al.*, 1997), and the Dudhia short-wave radiation scheme (Dudhia, 1989) are used. Figure 10 shows two-way nested domains and terrain height. The horizontal grid spacings for domains 1, 2, and 3 are 27, 9, and 3 km, respectively. The cumulus parametrization scheme is applied to domains 1 and 2. The numbers of horizontal grids for domains 1, 2, and 3 are 225×210, 225×210, and 354×390, respectively. The model top height is 50 hPa (~20 km). There are 42 stretched vertical layers, with a grid spacing of ~70 m in the lowest model layer. The 1-hourly $0.25° \times 0.25°$ resolution ERA5 reanalysis data (Copernicus Climate Change Service, 2017) are used for initial and boundary conditions. The model is integrated for 7 days and 12 hr starting from 1200 LST 16 June 2014, and the simulation results from 0000 LST 17 June to 0000 LST 24 June in the innermost domain are used for analysis (LST = UTC + 6 hr).

The simulated and observed 7-day accumulated precipitation amounts are shown in Figure 11. The spatial distribution of the accumulated precipitation amount is well simulated in NP, despite some underestimation. NP well predicts the large amount of precipitation over the southeastern region of Bangladesh. For the western region of Bangladesh, neither of the simulations manages to produce the observed amount of precipitation, but the prediction of NP is much closer to the observation than that of OP where the precipitation amount is more underestimated. Interestingly, OP largely overestimates (44%) the precipitation amount at Sylhet (24.90°N, 91.88°E) in the northeastern region of the country, while it is relatively well predicted by NP (overestimation by 10%).

Using the simulated and observed accumulated precipitation amounts at the location of each meteorological

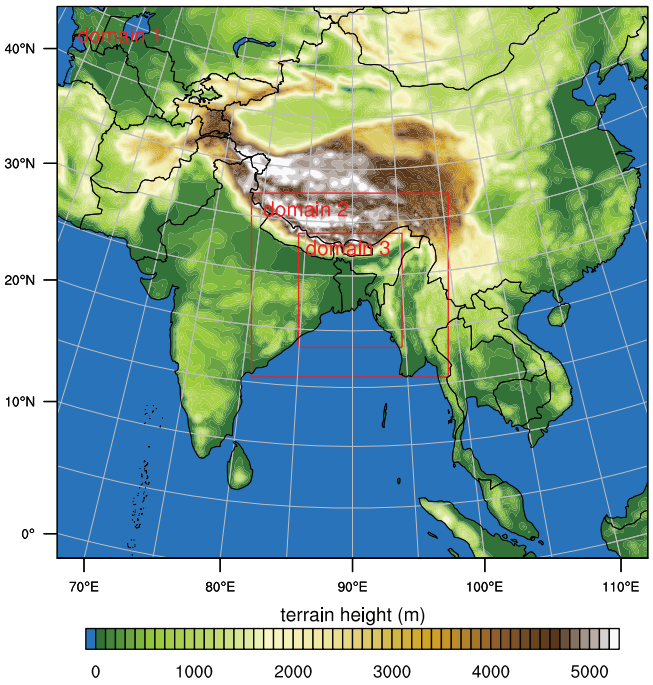

FIGURE 10 Three nested model domains for the real-case simulations and terrain height

station, Brier scores are calculated (Figure 12). For almost all precipitation thresholds, NP gives lower Brier scores than OP, which indicates better prediction of precipitation. The difference in Brier scores is pronounced for thresholds smaller than 200 mm and thresholds of 470–630 mm, owing to the better performance of NP in the western and the southeastern regions, respectively.

Figure 13 presents the time- and domain-averaged vertical profiles of hydrometeor mixing ratios and mass-weighted mean radii of raindrops and cloud droplets. Differences in the hydrometeor mixing ratio between the two accretion parametrizations are relatively small compared to those shown in the idealized simulations, possibly due to the long simulation period and the complicated dynamical environment of the real-case simulations. Among the hydrometeors, snow accounts for a large portion of clouds, indicating active ice microphysical processes. NP predicts a slightly larger snow mixing ratio at relatively low levels ($z \sim 5$–9 km) and a smaller snow mixing ratio at relatively high levels ($z \sim 9$–16 km), compared to OP. Mixing ratios of cloud water and rainwater are slightly smaller in NP than in OP, which can be attributed to the more active accretion process and the faster raindrop sedimentation in NP, respectively. Differences in the mean radii of raindrops and cloud droplets between NP and OP are evident. For $z \leq 5$ km, NP predicts 4% larger mean raindrop radius and 2% smaller mean cloud droplet radius. The larger (smaller) mean raindrop (cloud droplet)

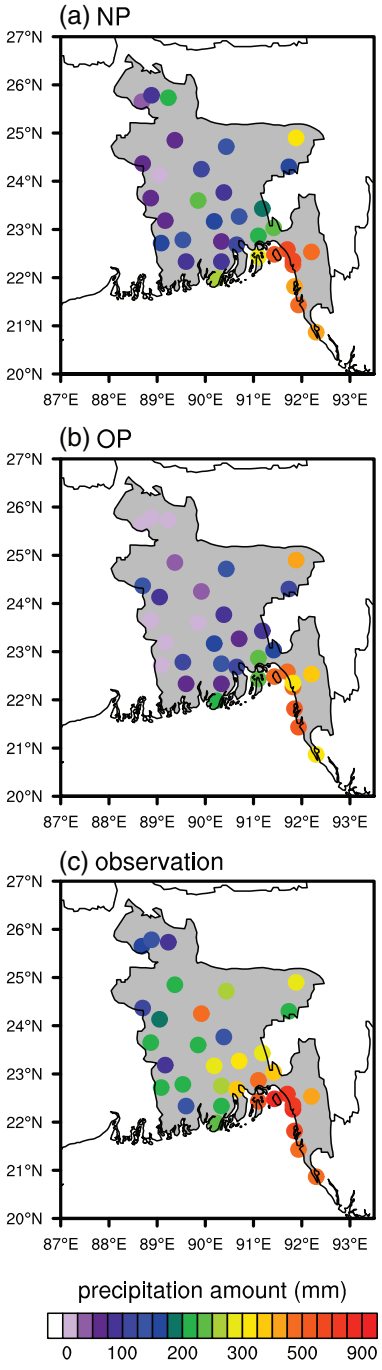

FIGURE 11 Spatial distributions of 7-day accumulated precipitation amount simulated with (a) NP and (b) OP and (c) observed at meteorological stations. The simulation results are interpolated to the locations of the meteorological stations in (a) and (b)

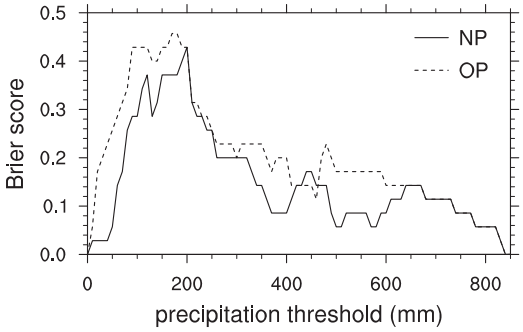

FIGURE 12 Brier scores calculated using the simulated and observed 7-day accumulated precipitation amounts at the location of each meteorological station

radius in NP is consistent with the result of the idealized simulations.

The effects of NP on the accretion and autoconversion rates are also very similar to those shown in the idealized simulations. Figure 14 shows the time series of domain-averaged accretion and autoconversion rates, where the domain average is taken both horizontally (the innermost domain) and vertically ($z = 0$–18 km). The time series in Figure 14, also in Figure 15, are plotted from 0000 LST 17 to 0000 LST 24 June 2014. In general, NP predicts a larger accretion rate and a smaller autoconversion rate than OP. The sum of the accretion and autoconversion rates shows little difference between NP and OP until 19 June when the precipitation rate was small, while the difference becomes large after that. The acc/auto ratio in NP is much higher than that in OP for the whole period, which is responsible for the larger mean raindrop radius in NP. The effects of NP on the liquid and ice water paths seem to be more complicated than those on the microphysical conversion rates (Figure 15). Notable differences in the water paths are found from 20 June. For 21–22 June, the two rainiest days in the simulation period, the liquid and ice water paths in NP are 4 and 8% larger than those in OP, respectively. The increases in the liquid and ice water paths lead to the increase in precipitation amount during this period, which results in the better precipitation prediction in NP.

The time- and domain-averaged vertical profiles of latent heating rates are shown in Figure 16. Although the differences in the latent heating rates between NP and OP for the real-case simulations are relatively small compared to those for the idealized simulations, important features of the differences such as stronger net latent heating via condensation and evaporation at low levels in NP that are shown in the idealized simulations are also found in the real-case simulations. The stronger latent heating in NP may to some extent have contributed to the larger precipitation amount. It is noted that the differences in the latent heating rates between NP and OP averaged over a 1-day period from 1800 LST (1200 UTC) 21 June when the difference in the accretion rate is largest are about seven times those averaged over the whole 7-day period.

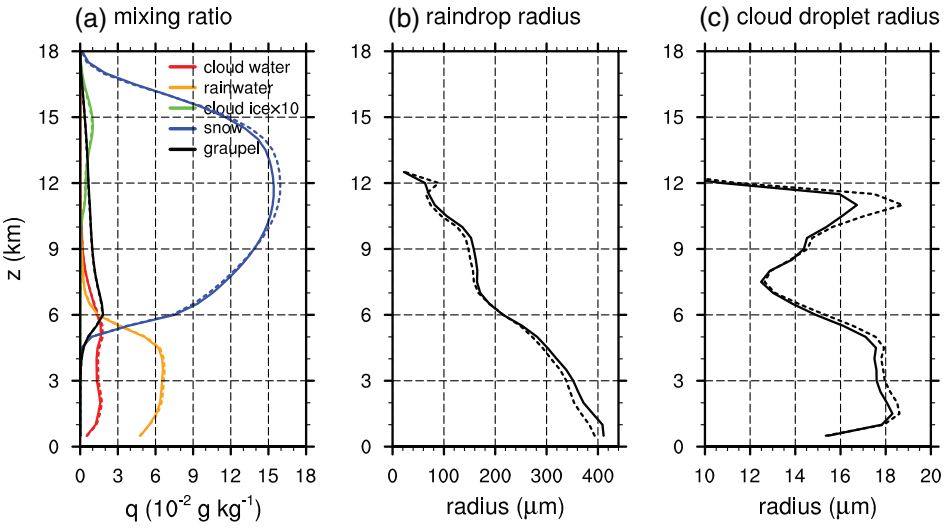

FIGURE 13 As in Figure 5, but for the real-case simulations

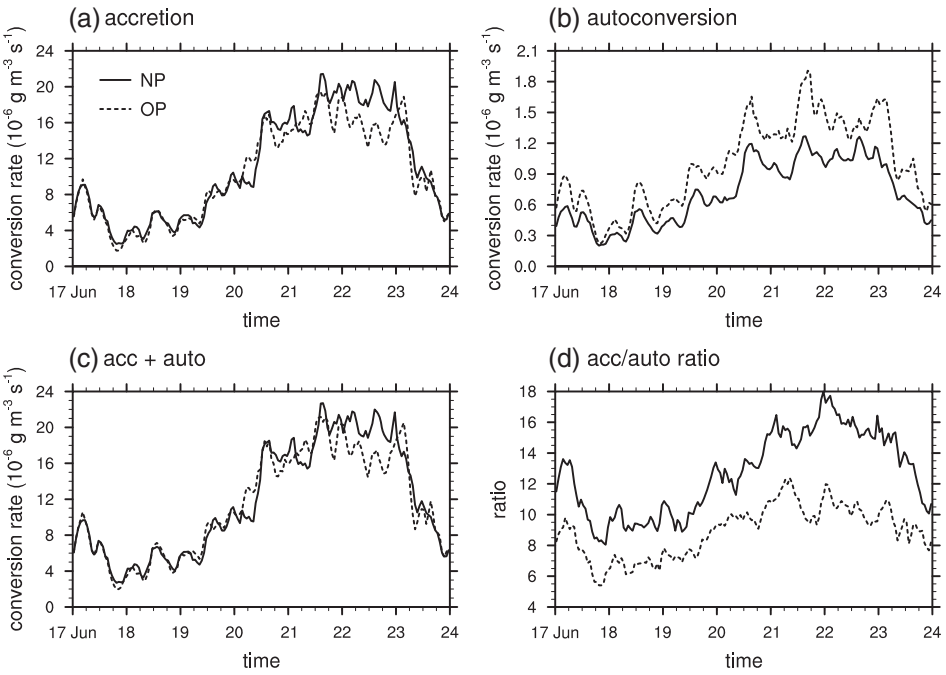

FIGURE 14 As in Figure 6, but for the real-case simulations (UTC + 6 hr, June 2014)

4 | SUMMARY AND CONCLUSIONS

Based on the stochastic collection equation, the accretion of cloud water by rainwater is newly parametrized for use in bulk microphysics schemes. The new accretion parametrization employs the collection efficiency of each raindrop–cloud droplet pair, which allows a strong variability of accretion rate depending on the cloud droplet and raindrop size distributions even for given cloud water and rainwater mass contents. In the idealized and real-case simulations using a cloud-resolving model, NP generally yields larger accretion rates and smaller autoconversion rates compared to OP, resulting in the high acc/auto ratio. The relatively large mean raindrop size in NP caused by the high acc/auto ratio affects the sedimentation and evaporation processes of raindrops. Stronger net latent heating by condensation and evaporation processes is found in NP, which may contribute to enhancement of the cloud development and precipitation. In the simulations of a real precipitation event over Bangladesh, NP predicts the accumulated precipitation amount and its spatial distribution that are closer to the observation.

The relatively complicated calculation for the accretion process in NP compared to that in OP accompanies the increase in the computational cost but only to a small degree. For the idealized simulations in Section 3.1 in which the cloud microphysics scheme is the only physics parametrization used, the simulation with NP costs total computation time ~2% longer than that of the simulation with OP. In the real-case simulations where the

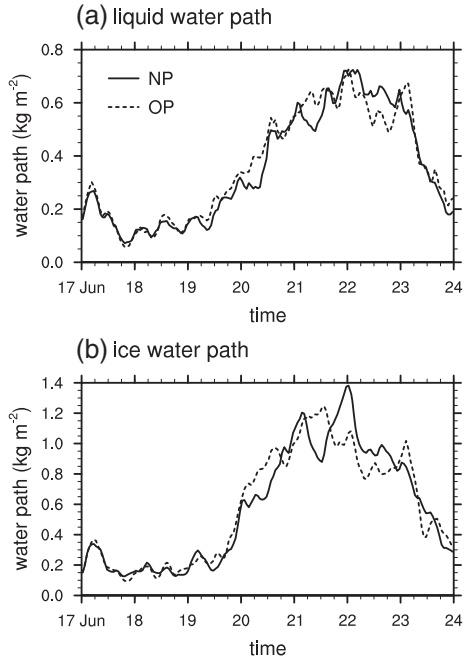

FIGURE 15 As in Figure 7, but for the real-case simulations (UTC + 6 hr, June 2014)

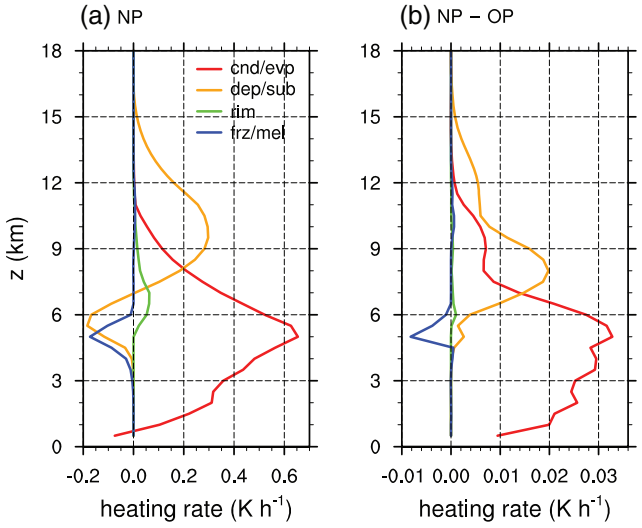

FIGURE 16 Time- and domain-averaged vertical profiles of (a) the heating rates due to condensation/evaporation, deposition/sublimation, riming, and freezing/melting in the real-case simulation with the new parametrization and (b) the differences in the heating rates between the new and original parametrizations

contribution of the cloud microphysics scheme to the total computational load is relatively small, the computation time is reduced further.

Although the new parametrization provides a more rigorous estimation of the accretion rate, there still are some uncertainties. The assumption that the coalescence efficiency is 1 is one of them. If the coalescence efficiency for the accretion regime in reality is much smaller than 1, the acc/auto ratio and the mean raindrop radius predicted by NP may have been overestimated. It is found that when the coalescence efficiency is assumed to be 0.75, the idealized simulation with NP still yields higher acc/auto ratio for a long time and overall greater raindrop radius than the idealized simulation with OP in which the coalescence efficiency is assumed to be 1, though differences in these variables between NP and OP are much reduced compared to those presented in Section 3.1. This implies that examining reliable coalescence efficiency through physically rigorous and reproducible experiments may be needed to further improve the accuracy of the accretion rate estimation.

The clouds simulated in this study to examine the effects of NP are mainly deep convective clouds with high liquid water path where the role of the accretion process is important (Michibata and Takemura, 2015). To see how these effects are different in shallow convective clouds with no ice microphysical processes involved, marine stratocumulus clouds are additionally simulated. The overall higher acc/auto ratio, larger mean raindrop radius, and smaller mean cloud droplet radius in NP than in OP are again predicted in these simulations, but the differences between those in NP and OP are not as big as the differences found in the deep convective cloud simulations, possibly because the importance of the accretion process relative to the autoconversion process is smaller compared to that in the deep convective cloud simulations (not shown).

The derivation of the accretion parametrization in this study shares many of the assumptions and methods with that of the autoconversion parametrization by LB17. Since the accretion and autoconversion processes are the two main processes that produce rainwater in warm clouds, coupling of the two parametrizations may improve the warm rain prediction, due to the elaborate methods used in the two parametrizations and a good consistency between them. It is expected that some of the effects of NP found in this study would be cancelled out and some would be amplified. For example, the LB17 parametrization predicts higher acc/auto ratio compared to many other autoconversion parametrizations (e.g. Berry and Reinhardt, 1974; Liu and Daum, 2004; Seifert and Beheng, 2006), and it will be worthwhile to examine how the high acc/auto ratio in NP will change when coupled with the LB17 parametrization. The combined effects of the two warm-rain collection parametrizations will be evaluated through simulations of various types of clouds and precipitation in further research. Furthermore, the parametrizations of the accretion processes involved with ice hydrometeors which share the methods with NP in this study (e.g. Jin *et al.*, 2019) can be also combined to better represent the collection processes in mixed-phase clouds.

ACKNOWLEDGEMENTS

The authors are grateful to two anonymous reviewers for providing valuable comments on this work. This work was supported by the Research Institute of Basic Sciences funded by the National Research Foundation of Korea (NRF-2019R1A6A1A10073437) and also by the Korea Meteorological Administration Research and Development Program under Grant KMI 2020-00710. The first author was supported by the SNU President Fellowship.

CONFLICT OF INTEREST

The authors declare no conflict of interest.

ORCID

Han-Gyul Jin https://orcid.org/0000-0001-5618-3529
Jong-Jin Baik https://orcid.org/0000-0003-3709-0532

REFERENCES

Beard, K.V. (1976) Terminal velocity and shape of cloud and precipitation drops aloft. *Journal of the Atmospheric Sciences*, 33, 851–864.

Beard, K.V. and Grover, S.N. (1974) Numerical collision efficiencies for small raindrops colliding with micron size particles. *Journal of the Atmospheric Sciences*, 31, 543–550.

Beard, K.V. and Ochs III, H.T. (1995) Collisions between small precipitation drops. Part II: Formulas for coalescence, temporary coalescence, and satellites. *Journal of the Atmospheric Sciences*, 52, 3977–3996.

Berry, E.X. and Reinhardt, R.L. (1974) An analysis of cloud drop growth by collection. Part II: Single initial distributions. *Journal of the Atmospheric Sciences*, 31, 1825–1831.

Cao, Q., Zhang, G., Brandes, E., Schuur, T., Ryzhkov, A. and Ikeda, K. (2008) Analysis of video disdrometer and polarimetric radar data to characterize rain microphysics in Oklahoma. *Journal of Applied Meteorology and Climatology*, 47, 2238–2255.

Copernicus Climate Change Service (C3S) (2017) ERA5: Fifth generation of ECMWF atmospheric reanalysis of the global climate. Copernicus Climate Change Service Climate Data Store (CDS). Available at: https://cds.climate.copernicus.eu/cdsapp#!/home [Accessed December 2019].

Dudhia, J. (1989) Numerical study of convection observed during the Winter Monsoon Experiment using a mesoscale two-dimensional model. *Journal of the Atmospheric Sciences*, 46, 3077–3107.

Dziekan, P. and Pawlowska, H. (2017) Stochastic coalescence in Lagrangian cloud microphysics. *Atmospheric Chemistry and Physics*, 17, 13509–13520.

Gaudet, B.J. and Schmidt, J.M. (2005) Assessment of hydrometeor collection rates from exact and approximate equations. Part I: A new approximate scheme. *Journal of the Atmospheric Sciences*, 62, 143–159.

Hong, S.-Y., Noh, Y. and Dudhia, J. (2006) A new vertical diffusion package with an explicit treatment of entrainment processes. *Monthly Weather Review*, 134, 2318–2341.

Janjić, Z.I. (1994) The step-mountain eta coordinate model: further developments of the convection, viscous sublayer, and turbulence closure schemes. *Monthly Weather Review*, 122, 927–945.

Jin, H.-G., Lee, H. and Baik, J.-J. (2019) A new parameterization of the accretion of cloud water by graupel and its evaluation through cloud and precipitation simulations. *Journal of the Atmospheric Sciences*, 76, 381–400.

Johnson, J.S., Cui, Z., Lee, L.A., Gosling, J.P., Blyth, A.M. and Carslaw, K.S. (2015) Evaluating uncertainty in convective cloud microphysics using statistical emulation. *Journal of Advances in Modeling Earth Systems*, 7, 162–187.

Kessler, E. (1969) *On the distribution and continuity of water substance in atmospheric circulations.* Meteorological Monographs 32. Boston, MA: American Meteorological Society.

Khain, A., Rosenfeld, D., Pokrovsky, A., Blahak, U. and Ryzhkov, A. (2011) The role of CCN in precipitation and hail in a mid-latitude storm as seen in simulations using a spectral (bin) microphysics model in a 2D dynamic frame. *Atmospheric Research*, 99, 129–146.

Khairoutdinov, M. and Kogan, Y. (2000) A new cloud physics parameterization in a large-eddy simulation model of marine stratocumulus. *Monthly Weather Review*, 128, 229–243.

Lee, H. and Baik, J.-J. (2017) A physically based autoconversion parameterization. *Journal of the Atmospheric Sciences*, 74, 1599–1616.

Lim, K.-S.S. and Hong, S.-Y. (2010) Development of an effective double-moment cloud microphysics scheme with prognostic cloud condensation nuclei (CCN) for weather and climate models. *Monthly Weather Review*, 138, 1587–1612.

Liu, Y. and Daum, P.H. (2004) Parameterization of the autoconversion process. Part I: Analytical formulation of the Kessler-type parameterizations. *Journal of the Atmospheric Sciences*, 61, 1539–1548.

Long, A.B. (1974) Solutions to the droplet collection equation for polynomial kernels. *Journal of the Atmospheric Sciences*, 31, 1040–1052.

Michibata, T. and Takemura, T. (2015) Evaluation of autoconversion schemes in a single model framework with satellite observations. *Journal of Geophysical Research – Atmospheres*, 120, 9570–9590.

Milbrandt, J.A. and Yau, M.K. (2005) A multimoment bulk microphysics parameterization. Part II: A proposed three-moment closure and scheme description. *Journal of the Atmospheric Sciences*, 62, 3065–3081.

Mlawer, E.J., Taubman, S.J., Brown, P.D., Iacono, M.J. and Clough, S.A. (1997) Radiative transfer for inhomogeneous atmospheres: RRTM, a validated correlated-k model for the longwave. *Journal of Geophysical Research*, 102(D14), 16663–16682.

Morrison, H., Curry, J.A. and Khvorostyanov, V.I. (2005) A new double-moment microphysics parameterization for application in cloud and climate models. Part I: Description. *Journal of the Atmospheric Sciences*, 62, 1665–1677.

Morrison, H. and Grabowski, W.W. (2007) Comparison of bulk and bin warm-rain microphysics models using a kinematic framework. *Journal of the Atmospheric Sciences*, 64, s 2839–2861.

Morrison, H. and Milbrandt, J.A. (2015) Parameterization of cloud microphysics based on the prediction of bulk ice particle properties. Part I: Scheme description and idealized tests. *Journal of the Atmospheric Sciences*, 72, 287–311.

Naumann, A.K. and Seifert, A. (2016) Evolution of the shape of the raindrop size distribution in simulated shallow cumulus. *Journal of the Atmospheric Sciences*, 73, 2279–2297.

Paukert, M., Fan, J., Rasch, P.J., Morrison, H., Milbrandt, J.A., Shpund, J. and Khain, A. (2019) Three-moment representation

of rain in a bulk microphysics model. *Journal of Advances in Modeling Earth Systems*, 11, 257–277.

Pinsky, M., Khain, A. and Shapiro, M. (2001) Collision efficiency of drops in a wide range of Reynolds numbers: effects of pressure on spectrum evolution. *Journal of the Atmospheric Sciences*, 58, 742–764.

Seifert, A. and Beheng, K.D. (2001) A double-moment parameterization for simulating autoconversion, accretion and selfcollection. *Atmospheric Research*, 59, 265–281.

Seifert, A. and Beheng, K.D. (2006) A two-moment cloud microphysics parameterization for mixed-phase clouds. Part 1: Model description. *Meteorology and Atmospheric Physics*, 92, 45–66.

Seifert, A., Blahak, U. and Buhr, R. (2014) On the analytic approximation of bulk collision rates of non-spherical hydrometeors. *Geoscientific Model Development*, 7, 463–478.

Skamarock, W.C., Klemp, J.B., Dudhia, J., Gill, D.O., Barker, D.M., Duda, M.G., Huang, X.-Y., Wang, W. and Powers, J.G. (2008) *A description of the Advanced Research WRF version 3. NCAR Technical Note TN-475+STR*. Boulder, CO: National Center for Atmospheric Research.

Straub, W., Beheng, K.D., Seifert, A., Schlottke, J. and Weigand, B. (2010) Numerical investigation of collision-induced breakup of raindrops. Part II: Parameterizations of coalescence efficiencies and fragment size distributions. *Journal of the Atmospheric Sciences*, 67, 576–588.

Tewari, M., Chen, F., Wang, W., Dudhia, J., LeMone, M.A., Mitchell, K., Ek, M., Gayno, G., Wegiel, J. and Cuenca, R.H. (2004) Implementation and verification of the unified Noah land surface model in the WRF model. *20th Conference on Weather Analysis and Forecasting/16th Conference on Numerical Weather Prediction, 12–16 January 2004*, Seattle, WA, pp 10–15.

Thompson, G. and Eidhammer, T. (2014) A study of aerosol impacts on clouds and precipitation development in a large winter cyclone. *Journal of the Atmospheric Sciences*, 71, 3636–3658.

Thompson, G., Field, P.R., Rasmussen, R.M. and Hall, W.D. (2008) Explicit forecasts of winter precipitation using an improved bulk microphysics scheme. Part II: Implementation of a new snow parameterization. *Monthly Weather Review*, 136, 5095–5115.

Tripoli, G.J. and Cotton, W.R. (1980) A numerical investigation of several factors contributing to the observed variable intensity of deep convection over south Florida. *Journal of Applied Meteorology*, 19, 1037–1063.

Walko, R.L., Cotton, W.R., Meyers, M.P. and Harrington, J.Y. (1995) New RAMS cloud microphysics parameterization. Part I: The single-moment scheme. *Atmospheric Research*, 38, 29–62.

Wood, R. (2005) Drizzle in stratiform boundary layer clouds. Part II: Microphysical aspects. *Journal of the Atmospheric Sciences*, 62, 3034–3050.

Wu, P., Xi, B., Dong, X. and Zhang, Z. (2018) Evaluation of autoconversion and accretion enhancement factors in general circulation model warm-rain parameterizations using ground-based measurements over the Azores. *Atmospheric Chemistry and Physics*, 18, 17405–17420.

How to cite this article: Ahmed T, Jin H-G, Baik J-J. A physically based raindrop–cloud droplet accretion parametrization for use in bulk microphysics schemes. *Q J R Meteorol Soc*. 2020;146:3368–3383. https://doi.org/10.1002/qj.3850